

# MODELLING ADHESION ENHANCEMENT IN WHEEL-RAIL CONTACT TRIGGERED BY SAND PARTICLES

Bin Zhang <sup>1,\*</sup>, Sadeh Nadimi <sup>1</sup>, Roger Lewis <sup>2</sup>

<sup>1</sup> School of Engineering, Newcastle University, Newcastle upon Tyne, NE1 7RU, United Kingdom

<sup>2</sup> Department of Mechanical Engineering, The University of Sheffield, Mappin Street, Sheffield, S1 3JD, United Kingdom

\* E-mail: B.Zhang48@newcastle.ac.uk

**Abstract:** Sanding is widely used in train operation to enhance the adhesion level in both braking and acceleration conditions. By employing cohesive interface elements (CIEs), a finite element method (FEM) is developed in this study to explore the adhesion enhancement triggered by sand particles. A wheel-rail model is developed and four different particle sizes are selected to observe the influence of fracture behaviour on the traction before and after the particle breakage. The coefficient of traction from the simulations are calculated and analysed. The results indicate that the adhesion enhancement is not affected by particle size, but the amount of fragments generated and the coefficient of traction is induced by wheel rolling on particle fragments.

**Keywords:** wheel-rail adhesion; particle breakage; particle size; cohesive interface element.

## 1. Introduction

Adhesion in the wheel-rail contact significantly influences the braking distance and train traction [1]. Poor adhesion causes longer stopping distance and reduced train acceleration. In a case of loss of adhesion, sand particles are fired at the contact from an on-board device to enhance the adhesion level. Sanding is a widely adapted practice in most railway networks. It usually occurs automatically during emergency braking, but is a manual process for control of traction.

Several researchers have investigated the adhesion enhancement and restoration affected by sanding application [1, 2]. The effect of particles on adhesion and leaf layer removal, as well as the traction enhancers have been analysed using twin-disc set-up, linear full-scale rig and field tests [1]. Sand entrainment analysis related to hose type, hose position and crosswind have been carried out experimentally to optimise the railway sanding system [2]. All these studies explain well the advantages and limitations of sanding in railways.

The Rail Safety and Standards Board (RSSB) standard GMRT2461 [3] specifically defines the size distribution and shape characteristics of sand for braking and traction. Operational experience has shown that a coarse particle size sand is more suitable for braking while fine particle size is more suitable for acceleration [3]. Additionally, the magnitude of adhesion enhancement is correlated to particle size [4, 5]. An investigation on the role of particle size on the likelihood of isolation revealed that fine and medium-sized sand particles (0.06–0.3mm and 0.3–0.6

mm, respectively) are more likely to cause isolation [6]. They suggested that this might be due to smaller particles not breaking-up and being ejected upon entering the contact, thus allowing a layer of sand to build-up. Shi et al. [7] used a twin-disc set-up to analyse the particle-size effects based on standard sand and its micro-fragments. They found that the micro-fragments enhance adhesion at a smaller cost of wheel-rail wear and damage. While it is clear that initial particle size and how the particles break-up at the wheel-rail interface are influential on traction enhancement as well as possible damage to wheel and rail, there is little research on the exact physical mechanisms that occur as the sand is entrained.

In this study, a wheel-rail model is developed using the finite element method to study the influence of sand particle breakage on wheel traction systematically. Four different particle sizes were selected based on the RSSB standard GMRT2461 [3] and used to observe the influence of fracture behaviour on the traction in the wheel-rail contact before and after the particle breakage. A full-scale wheel was created with boundary conditions assigned to reproduce real wheel-rail contact conditions. The coefficient of traction from four tests were calculated and analysed. This study provides new insights into the effect of particle size and its fracture behaviour for railway sanding systems. The method used in this study will provide a procedural framework for other studies.

## 2. Material and Method

Four circular particles were meshed, using a constant element size, representing 0.71 mm, 1 mm, 2 mm and 2.8 mm diameter particles. The element size was kept constant as it controls the minimum size of the fragments after breakage. Cohesive interface elements (CIEs) were inserted between each element for breakage simulations. Based on governing equations, particles can break and fracture can propagate at the element interface. In this section, the governing laws of CIE are briefly presented and the detail of the numerical model is described.

### 2.1. Cohesive Interface Elements

Among many approaches to simulate fracture behaviour, CIEs is one of the most popular methods that can simulate material debonding effectively [8]. After a mesh is generated, CIEs are inserted at every element edges. Since the CIE is zero-thickness, the geometry of the mesh has not been changed but every element now is bonded by the CIE. When the normal stress or shear stress at the CIE is reaching a threshold value, the CIE starts to vanish

thus debonding between elements occurs. This behaviour of CIE can be illustrated by the bi-linear cohesive traction-separation law [9], as shown in Figure 1. The traction stress vector,  $\sigma$ , consists of normal and two shear components:

$$\sigma = \begin{pmatrix} \sigma_n \\ \sigma_s \\ \sigma_t \end{pmatrix} = K \delta = \begin{pmatrix} k_{nn} & k_{ns} & k_{nt} \\ k_{sn} & k_{ss} & k_{st} \\ k_{tn} & k_{ts} & k_{tt} \end{pmatrix} \begin{pmatrix} \delta_n \\ \delta_s \\ \delta_t \end{pmatrix} \quad (1)$$

where  $K$  is the elasticity matrix,  $\delta$  is the relative displacement matrix, and  $n$ ,  $s$  and  $t$  denote the normal and two shear directions.

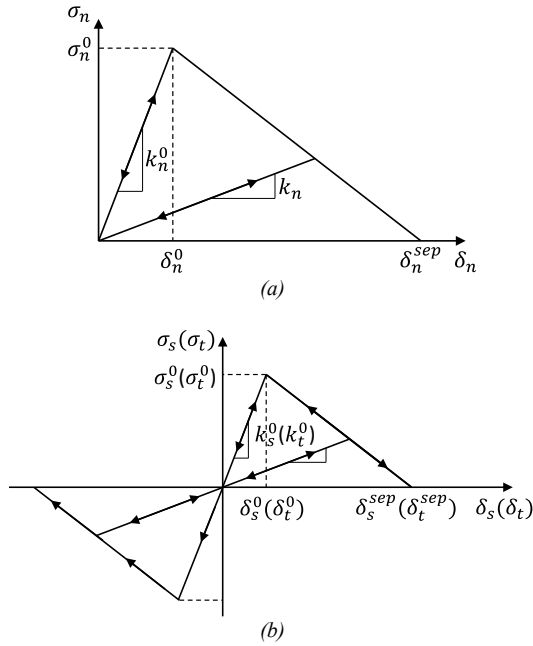


Figure 1 Bi-linear cohesive traction-separation law: (a) normal component, (b) shear component.

## 2.2. Numerical Model

Two discrete frictionless rigid parts were created in Abaqus finite element software package to represent a wheel and rail. The wheel was assigned with a displacement in the X direction (ca. 100 mm) and a rotation at 20 MPH, with a 70 kN concentrated force at the centre. The rail was constrained by a fixed boundary condition to limit the motion from all directions. The layout of the finite element model is illustrated in Figure 2; where the inset shows a zoomed view of a particle.

Here, particles are assumed to be circular and the diameter changes from 0.71 mm to 2.8 mm according to the RSSB standard GMRT2461 [3, 5]. All particles were generated using 3-node linear plane strain triangle (CPE3) elements. A constant element size of 0.1 mm was assigned for all particle meshes in order to limit the minimum fragment size regardless of the particle size, as shown in Figure 3. This allows direct comparison between different particle sizes. Cohesive elements (COH2D4) were inserted between CPE3 elements by employing an open-source software developed by Zare-Rami & Kim [8].

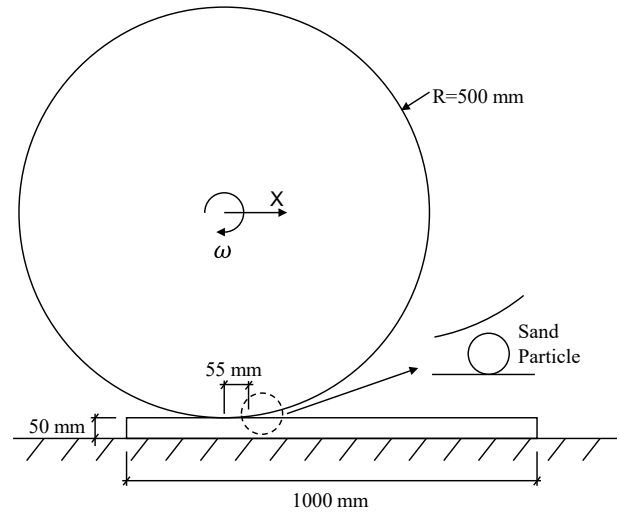


Figure 2 Schematic diagram of the Finite Element model.

Since the COH2D4 elements have zero in-plane thickness, the mesh geometry is not changing. Each individual element can locally deform depending on the current nodal forces and the traction-separation relation allows crack initiation and propagation where CIE exists. The body motion in the simulation is calculated using an explicit central difference integration rule.

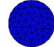
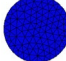
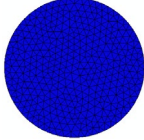
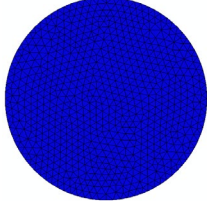
	Mesh size (mm)	Element size (mm)	CPE3 element
	0.71	0.1	92
	1	0.1	179
	2	0.1	733
	2.8	0.1	1399

Figure 3 Different particle sizes.

Material parameters of quartz sand particles were selected to investigate the fracture behaviour in a geotechnical material. Table 1 summarises the material parameters used in this study, including density ( $\rho$ ), elastic modulus ( $E$ ), Poisson's ratio ( $\nu$ ), tensile strength ( $N_{max}$ ) and shear strength ( $S_{max}$  and  $T_{max}$ ) and CIEs stiffness ( $k_n$ ,  $k_s$  and  $k_t$ ), fracture energy ( $G_n$ ,  $G_s$  and  $G_T$ ) and material parameter ( $\eta$ ). These parameters are referenced from Zhang et al. [10] and were calibrated to produce the best fit with the experiment.

**Table 1** FEM Material parameters used in this study.

Solid Elements		
Density	$\rho$ ( $kg/m^3$ )	2500
Young's Modulus	$E$ (GPa)	63
Poisson's ratio	$\nu$	0.22
Cohesive interface elements (CIEs)		
Normal stiffness	$k_n$ (N/mm <sup>2</sup> )	63000
First shear stiffness	$k_s$ (N/mm <sup>2</sup> )	31500
Second shear stiffness	$k_t$ (N/mm <sup>2</sup> )	31500
Tensile strength	$N_{max}$ (MPa)	25
First shear strength	$S_{max}$ (MPa)	12
Second shear strength	$T_{max}$ (MPa)	12
Mode I fracture energy	$G_n$ (N/mm)	0.1
Mode II fracture energy	$G_s$ (N/mm)	0.2
Mode III fracture energy	$G_t$ (N/mm)	0.2
Material parameter	$\eta$	2
Contact law		
Particle-to-Structure friction coefficient	$\mu$	0.3

### 3. Result and Discussion

In this section, we focus on statistical analysis and results correlating fragments distribution and coefficient of traction triggered by sand particle breakage at the wheel-rail contact.

#### 3.1. Particle Fragment Distribution

Based on the particle state during the simulation, the fracture process is divided into three stages: 1) prior-to-fracture, when the wheel is moving towards the particle; 2) fracture stage, where the first contact is happening, followed by multiple contacts. During this stage, the particle breaks into fragments; 3) post-fracture stage, where the wheel is rolling on top of fragments. The illustrative images for the different stages are given in Figure 4. Figure 4(a) shows the intact particle before breakage. Figure 4(b) shows stress concentration at the points of contacts between wheel-particle and particle-rail. Figure 4(c) shows chipping of the particle and Figure 4(d) shows fragmentation and the wheel rolling on the fragments.

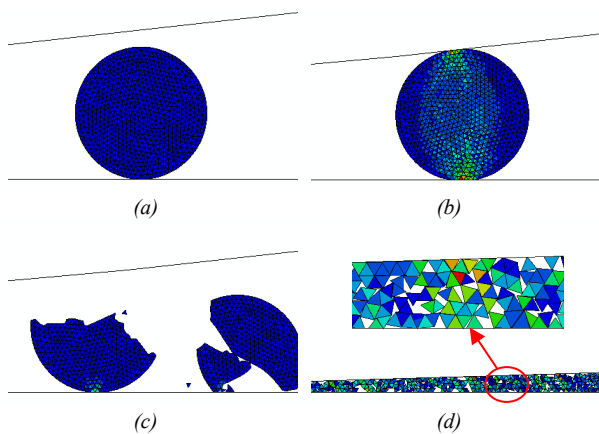
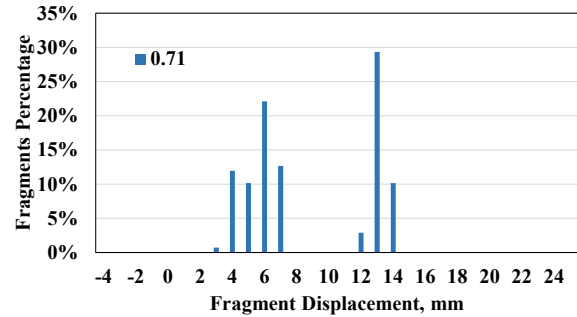
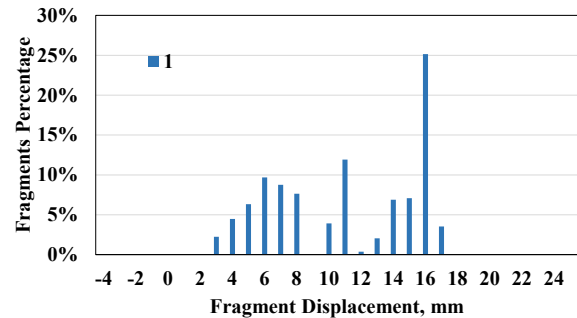


**Figure 4** Particle Images before and after breakage: (a) prior-to-fracture, (b) fracture stage-sliding, (c) fracture stage-breakage, (d) post-fracture stage.

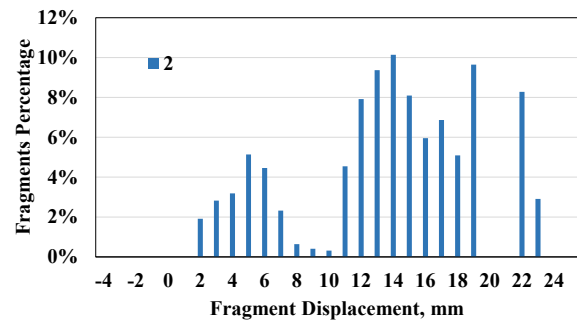
After particle fragmentation, the element size fragments are spread along the rail. Figure 5 shows the histogram of fragment percentage against their locations for different particle sizes. The zero on the X axis indicates the initial location of particle element before breakage. The fragments of minimum element dimension (0.1 mm) from coarser particles (i.e., diameter 2 and 2.8 mm) are well spread along the rail, while the ones from finer particles (i.e., diameter 0.71 and 1 mm) show 'patchy' spread.



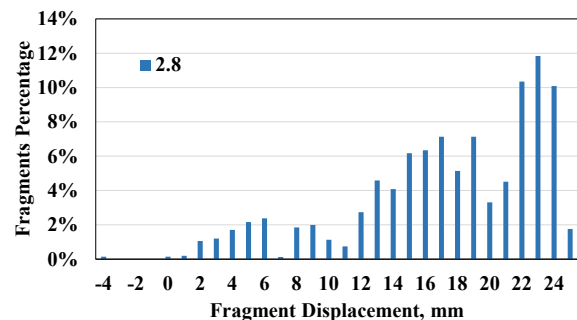
(a)



(b)



(c)



(d)

**Figure 5** Particle fragment distribution: (a) particle diameter 0.71 mm, (b) particle diameter 1 mm, (c) particle diameter 2 mm, (d) particle diameter 2.8 mm.

### 3.2. Coefficient of Traction

During the simulation set-up, a 70 kN concentrated force is assigned to the centre of the wheel, which is a typical load for a passenger train [11]. The tangential force along the moving direction is recorded through the entire simulation. The wheel-rail contact was assumed to be frictionless, however, the coefficient of friction between fragment-to-wheel and fragment-to-rail and fragment-to-fragment were set to 0.3. The overall traction came from these micro frictional contacts and interlocking of the fragments. To compare this with experimental data, the traction from dry wheel-rail contact needs to be subtracted from the enhanced traction. Therefore, the coefficient of traction can be quantified using the equation below:

$$\mu = F/N \quad (2)$$

where  $\mu$  is the coefficient of traction,  $F$  is tangential force and  $N$  is the normal force.

#### 3.2.1. The Effect of Predefining Contact Gap

The simulation will not be stable if the numerical elements are subjected to a high level of distortion. Before investigating different methods to control mesh distortion, a geometrical gap can be predefined in the numerical model, small enough to only avoid excessive element distortion. A gap with 0.1, 0.12, 0.15 and 0.2 mm thickness was introduced in the numerical model between wheel and rail. A 1 mm diameter particle was used in all simulations. The coefficient of traction for the system was computed.

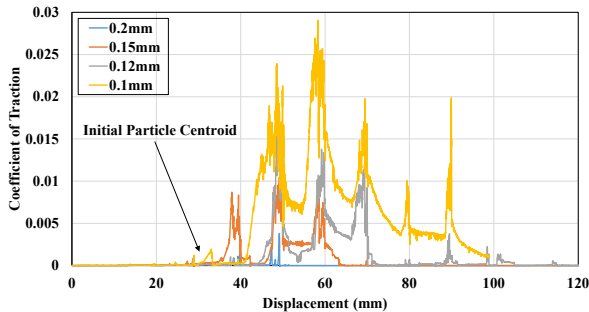


Figure 6 Coefficient of traction for different wheel-rail gaps

The calculated coefficient of traction for different wheel-rail gaps are showed in the Figure 6. The first contact is occurring earlier when the gap is decreasing, but the variation trend of the coefficient of traction for different gaps are similar. When the gap is bigger than the element size, the particle is partially fractured until the gap equals to the element size, then the particle is fully fragmented. Thus, the bigger gap causes a lower coefficient of traction and finishes the fracture process in a short period of time, whereas the smaller gap contributes to a higher coefficient of traction and takes longer time to complete the fracture process. However, a gap smaller than the element size leads to serious element distortion with longer computation time. Therefore, a gap equals to the minimum element dimension (0.1 mm) was selected to simulate the phenomenon that wheel is rolling on top of the sand powder layer.

#### 3.2.2. Element Distortion Control

By employing the CIEs, the bounded CPE3 elements are able to separate at the pre-defined threshold. However, the deformation of each single element is not trivial to control due to hard contact and high force transmission between elements, within a short period of time. This may lead to a simulation failure caused by element distortion. Therefore, four different element control methods naming no mesh control, element deletion & max degradation (E&D), distortion control and Arbitrary Lagrangian Eulerian (ALE) adaptive mesh domain were compared to optimize the simulation.

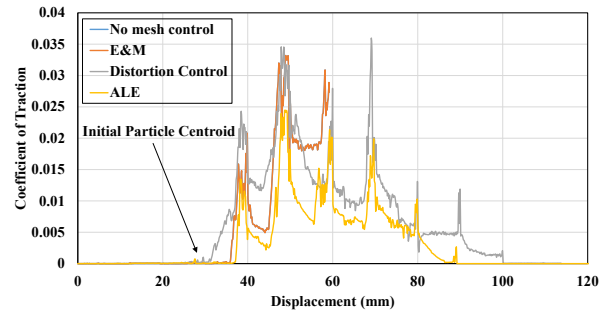


Figure 7 Coefficient of traction for different mesh control methods

Overall, the variation trend of coefficient of traction for different methods are similar, as shown in Figure 7. The E&M method is not providing any improvements from the no mesh control as the plots from these two methods are overlapping and both simulations failed at 60 mm. The distortion control method presents a great advantage as the variation trend of the coefficient of traction can be fully observed and the simulation terminated at 110 mm. The simulation using ALE adaptive mesh domain has been finished completely and the observed coefficient of traction stops at 90 mm, which is 10 mm less than the distortion control method. The ALE adaptive mesh domain method is utilized in this study due to less computation cost.

#### 3.2.3. Particle Size Analysis

The results for different particle sizes are shown in Figure 8. Since the particle centroid was placed 55 mm away from the wheel, the locations of first contact for each particle slightly varied due to the size difference. During the first contact, the generated coefficient of traction for all particles was small when compared with the values at post-fracture stage. After the first contact, the coefficient of traction starts to increase due to the particle breakage, which generates fragments. When the wheel reaches the initial particle centroid at 55 mm, the particle is fully fractured and the wheel is rolling on fragments. At this point the coefficient of traction increased sharply, as showed in Figure 6. The variation trends of coefficient of traction observed for different particles are similar, but the magnitude grows when the particle size increases. The experimental data reported in [5] show an increase of coefficient of traction from 0.01 to 0.4. The values obtained in this study (ranging from 0.003 to 0.1) can be related to initial shape of the particles.

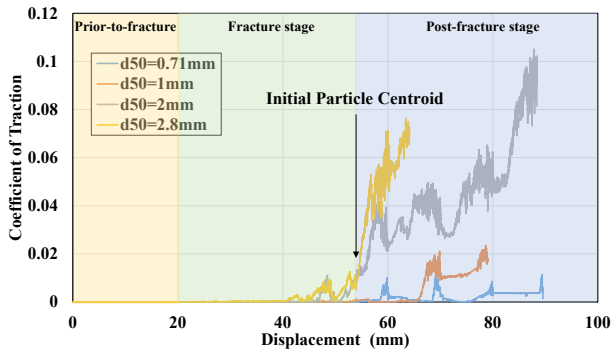


Figure 8 Coefficient of traction for single particle with varied diameters.

Since the element size of 0.1 mm was assigned to all the particles, the number of fragments generated during the wheel-rail contact varies from particle to particle. Therefore, a normalised coefficient of traction has been plotted to investigate adhesion enhancement from a newly generated surface area. As shown in Figure 9, the adhesion enhancement triggered by sand can be correlated to the number of generated fragments, in other words, adhesion enhancement is caused by the newly generated surface area of the third body. This observation needs to be confirmed by running extra simulations, considering the effect of particle shape and running experiments in which the amount of fragments can be controlled.

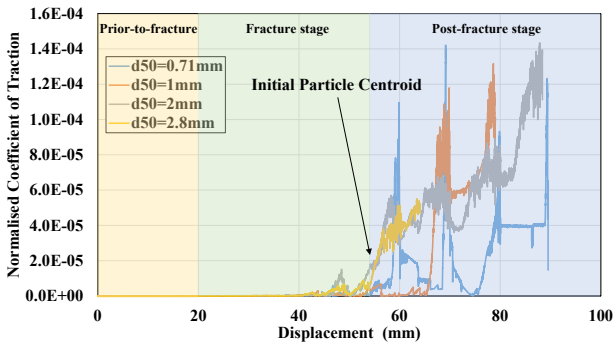


Figure 9 Normalised coefficient of traction for single particle with varied diameters.

### 3.2.4. Multi-particles Analysis

Since the single particle simulations for different particle sizes prove the adhesion enhancement from the dry wheel-rail contact, the next step is to simulate the multi-particles condition and its objective is twofold: (a) to find out the effective length for each particle, as upon fragmentation a particle covers a certain length of the rail, (b) to design the application rate of the sanding system according to the particle size and their effective length.

Following the previous set-up, two 1 mm particles were placed on the rail with a 100 mm distance in between. The particle centroid of the first particle was 30 mm away from the wheel, as showed in the Figure 8. All the material properties and modelling conditions were kept the same from the single particle simulation.

The fracture behaviour of the two particles are similar and the calculated coefficient of traction for the entire simulation is plotted in the Figure 10. The coefficient of

traction for the first particle starts to change at the location of initial particle centroid (30 mm) and ends at 100 mm, with a highest value of 0.027. A comparable coefficient of traction has been captured for the second particle that begins to increase at its initial particle centroid (130 mm) and backs to zero at 190 mm, with a highest value of 0.022. The mentioned variation trend and highest value are identical to the ones in single particle simulation. The coefficient of traction for multi-particles is a duplication of the coefficient of traction for single particle, when the space in between particles is bigger enough. Therefore, the targeted coefficient of traction can be maintained by placing sand particles at certain spacing. This conclusion needs to be further confirmed by running additional parametric multi-particles simulations with different spacing.

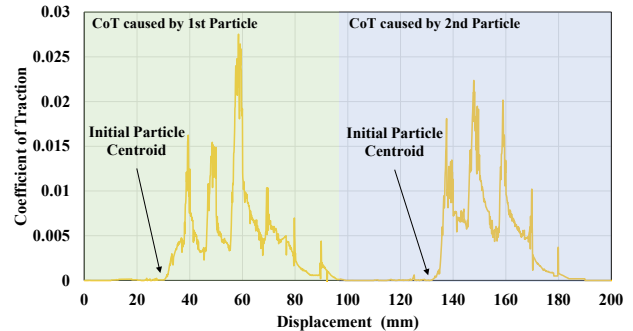


Figure 10 Coefficient of traction for multi-particles.

## 4. Conclusions and Future Study

Four different particle sizes have been selected according to the RSSB standard catalogue and tested in a simulated wheel-rail contact using a finite element method to investigate the particle breakage behaviour and size effects on enhancing adhesion. The only distinct difference between the particles was in their sizes. The simulation results demonstrated that all particles had small impact on the traction at the first contact with the wheel. All particles started to improve the traction when the wheel was rolling on their fragments. The bigger particle size generated more fragments ending with a higher coefficient of traction. However, this difference between particles became negligible when the coefficient of traction is normalised by the number of fragments which can be correlated to newly generated surfaces. This allows uncoupling of the effect of particle size from the newly generated surface area. A multi-particles simulation was also performed using a single particle size. It validated the coefficient of traction calculated from single particle simulations and provided an initial guidance for spacing the particles to achieve a targeted adhesion level.

As a preliminary study to investigate the adhesion enhancement induced by sand particle breakage at the wheel-rail contact, simplifications were made to run the simulations. By using the particle classification system and image processing technology, extra efforts will be given to quantify the shape effect from initial particle and its fragments to the adhesion enhancement. The quantified results will be further validated by running

experiments in which the shape of sand particles and the amount of fragments can be controlled.

### Acknowledgments

The first author is funded by China Scholarship Council – Newcastle University Scholarships (CSC-NU). The authors acknowledge the support of the UK Engineering and Physical Sciences Research Council (EPSRC), grant number EP/V053655/1.

### References

- [1] Skipper, W.A., Chalisey, A. and Lewis, R., 2018. A review of railway sanding system research: adhesion restoration and leaf layer removal. *Tribology-Materials, Surfaces & Interfaces*, **12**(4), pp.237-251.
- [2] Lewis, S.R., Riley, S., Fletcher, D.I. and Lewis, R., 2018. Optimisation of a railway sanding system for optimal grain entrainment into the wheel–rail contact. *Proceedings of the Institution of Mechanical Engineers, Part F: Journal of Rail and Rapid Transit*, **232**(1), pp.43-62.
- [3] Rail Safety and Standards Board, “GMRT2461 Sanding Equipment (Issue 3).” pp. 1–24, 2018.
- [4] Cooper (1972). An investigation into the relationship between the Particle Size and the Frictional Performance of Sand (IM-ADH-011) British Rail Report.
- [5] Skipper, W.A., Nadimi, S., Chalisey, A. and Lewis, R., 2019. Particle characterisation of rail sands for understanding tribological behaviour. *Wear*, **432**, p.202960.
- [6] Arias-Cuevas, O., Li, Z. and Lewis, R., 2010. Investigating the lubricity and electrical insulation caused by sanding in dry wheel–rail contacts. *Tribology Letters*, **37**(3), pp.623-635.
- [7] Shi, L.B., Wang, C., Ding, H.H., Kvarda, D., Galas, R., Omasta, M., Wang, W.J., Liu, Q.Y. and Hartl, M., 2020. Laboratory investigation on the particle-size effects in railway sanding: Comparisons between standard sand and its micro fragments. *Tribology International*, **146**, p.106259.
- [8] Zare-Rami, K. and Kim, Y.R., 2019. MIDAS-VT-Pre: Software to generate 2D finite element model of particle/fiber embedded composites with cohesive zones. *SoftwareX*, **10**, p.100292.
- [9] Wei, D., Zhao, B., Dias-da-Costa, D. and Gan, Y., 2019. An FDEM study of particle breakage under rotational point loading. *Engineering Fracture Mechanics*, **212**, pp.221-237.
- [10] Zhang, B., Nadimi, S., Eisa, A., and Rouainia, M., 202X. Modelling fracturing process using cohesive interface elements: theoretical verification and experimental validation. *Computational Particle Mechanics*, (JCPM-D-22-00095).
- [11] Mazzù, A., Ghidini, A., Zani, N. and Faccoli, M., 2021. A simplified numerical study of wheel/rail material coupling in presence of solid contaminants. *Tribology-Materials, Surfaces & Interfaces*, **15**(2), pp.102-114.